Implementation of “Blade material behavior under complex stress states” in technical standards

OB_TG2_R027_ rev. 000

Version 1
Confidential

OPTIMAT BLADES

TG2

Theodore P. Philippidis

UNIVERSITY OF PATRAS · TU Delft · DLR · VUB · ECN · KAPE CRES

Change record

Issue/revision	date	pages	Summary of changes
Version 1	13-7-2006	NA	NA

ACKNOWLEDGEMENT

Research funded in part by European Commission in the framework of the specific research and technology development programme Energy, Environment and Sustainable Development.

The Research performed by University of Patras is funded in part by the General Secretariat for Research & Technology, Ministry of Development. Project number: FK-6660

Table of Contents

1. Summary

A brief account of results from the work performed in TG2 is presented herein. Special emphasis is given in issues that could influence or affect design guidelines for rotor blades. This report summarizes the contribution from TG2 to the document of TG6 “Implementation of OPTIMAT in Technical Standards”.

2. In-plane static and fatigue test program

In the frame of TG2, a comprehensive experimental program was performed to fully characterize the in-plane behavior of UD material. To this end a number of at least 25 tests per category were performed, to have a statistical description as well, for measuring the following engineering constants:

E_1: Modulus of elasticity in the fiber direction
E_{1C}: Compressive modulus of elasticity in the fiber direction
E_2: Modulus of elasticity transverse to the fiber
E_{2C}: Compressive modulus of elasticity transverse to the fiber
G_{12}: In-plane shear modulus
v_{12}: Major Poisson ratio
v_{21}: Minor Poisson ratio
X_T: Tensile strength in the fiber direction
X_C: Compressive strength in the fiber direction
Y_T: Tensile strength transverse to the fiber
Y_C: Compressive strength transverse to the fiber
S: In-plane shear strength
ε_{1T}: Tensile failure strain in the fiber direction
ε_{1C}: Compressive failure strain in the fiber direction
ε_{2T}: Tensile failure strain transverse to the fiber
ε_{2C}: Compressive failure strain transverse to the fiber
γ_{S12}: In-plane shear strain at failure
α_1: Thermal expansion coefficient in the fiber direction
α_2: Thermal expansion coefficient transverse to the fiber

All experiments were performed at the same lab (UP), same test rig, same procedures so as to minimize variations in material property. Test coupons were delivered directly by LM. Test methods and detailed results were presented in a number of OPTIMAT reports [OB_TG2_R013], [OB_TG2_R018], [OB_TG2_R020].

In addition, a comprehensive experimental program for fatigue characterization of the UD material was performed in TG2 including definition of S-N curves at three R-ratios, 0.1, -1 and 10, both in the fiber and the transverse direction as well as in-plane shear fatigue strength under R=0.1. Standard S-N definitions from these tests are included in [OB_TC_R014, rev.005] while detailed test methods and results are presented in [OB_TG1_R013], [OB_TG2_R020], [OB_TG2_R021].

In all static and fatigue tests, except for in-plane shear characterization tests which were based on ISO 14129 geometry and test method, the standard OB coupon geometry was used, introducing the concept for just one geometry coupon valid for all types of tests, e.g. static or fatigue in tension and compression, residual strength etc. Only thickness was varying from coupons tested in the fiber direction to those loaded transversely to the fiber. Results are presented in Table 1. R_k(5%, 95%) denotes characteristic property value corresponding to the 5% fractile and 95% lower confidence limit in the mean value of the sample.

Most of the above cited mechanical properties were also measured in TG3 using ISO based test methods and coupon geometries [OB_TG3_R007]. Comparison of the two sets of values is presented in Table 2. As it is seen, values for strength and moduli are in very good agreement except the compressive strength in the fiber direction where the OPTIMAT specimen performs not so well due to bending deformation. Strains at failure present greater differences but it can be

argued that in general the OB standard coupon geometry for UD is a viable approach to complete in-plane material characterization.

Concerning in-plane shear strength and modulus, a detailed comparison of several different methods and standards was presented in [OB_TG2_R023] showing large discrepancies in test results. It seems that the method selected in TG2, i.e. ISO 14129, tensile test of $[\pm 45]_S$ laminated coupon yields fair results concerning both the shear modulus and strength. Perhaps, a modification of this standard would be to allow for somehow greater shear strength, S, values, e.g. instead of calculating S equal to half the tensile strength, $S = \sigma_{T_{45}} / 2$, of the $[\pm 45]_S$ coupon, accepting, as a rule of thumb, a value of shear strength equal to $S = \sigma_{T_{45}} / \sqrt{3}$.

S-N curve definitions for in-plane CA cyclic loading, at various R values, along the fiber direction, transversely or in shear are presented in Table 3. σ_a or τ_a stand for normal or shear stress amplitude respectively. Corresponding constant life diagrams are shown in Fig.1.

Table 1. In-plane mechanical and thermal property values of OPTIMAT UD material

	in GPa							in $^oC^{-1}$	
Statistics	**E1**	**E1c**	**E2**	**E2c**	**G12**	**v12**	**v21**	**a_1**	**a_2**
Min	36.74	37.44	13.54	14.41	4.032	0.24	0.0836	5.42E-06	1.88E-05
Max	41.38	40.1	14.73	15.65	4.396	0.3459	0.1075	1.17E-05	2.76E-05
Mean	39.04172	38.865	14.0772	14.99769	4.238792	0.290576	0.095036	9.17E-06	2.35E-05
Std. Dev.	1.032335	0.581985	0.324789	0.254909	0.099173	0.027137	0.006456	1.53E-06	2.08E-06
Valid Obs.	29	26	25	26	24	29	25	2.50E+01	2.50E+01
COV%	2.644183	1.497452	2.307196	1.699653	2.339644	9.339083	6.793212	16.70985	8.87523
R_k(5%, 95%)	37.02859	37.72986	13.43588	14.49613	4.042364	0.23765	0.082292	6.14E-06	1.93E-05

	in MPa									
Statistics	**X**	**X'**	**Y**	**Y'**	**S**	**ε_{1T} %**	**ε_{1c} %**	**ε_{2T} %**	**ε_{2c} %**	**γ_{S12} %**
Min	695.03	-541.58	49.58	-171.69	54.04	1.898	-1.598	0.3531	-2.2633	2.852
Max	836.03	-480.82	59.92	-148.98	57.81	2.355	-1.274	0.4875	-1.637	3.974
Mean	776.4972	-521.8219	53.9516	-165.0042	56.08	2.091276	-1.406038	0.421568	-1.997746	3.388667
Std. Dev.	36.14304	16.50091	2.576446	4.848872	1.119055	0.095839	0.069373	0.037564	0.165585	0.289422
Valid Obs.	29	26	25	26	25	29	26	25	26	24
COV%	4.654625	3.162173	4.775476	2.938635	1.995461	4.582788	4.933926	8.91063	8.288577	8.540868
R_k(5%, 95%)	706.0043	-489.3545	48.82434	155.4616	53.85296	1.9043	-1.27	0.3474	-1.672	2.8154

Table 2. Comparison of UD properties derived from ISO and OPTIMAT test coupons

	ISO	C.O.V%	OPTIMAT	C.O.V%	% differ.
Young mod. In the fiber direction, E_1 [GPa]:	39.01	8.818	39.04	2.644	-0.0769
Compr. mod. In the fiber direction, E_{1c} [GPa]:	39.31	4.172	38.865	1.497	1.1320
Young mod. In the transverse dir. E_2 [GPa]:	15.15	5.148	14.0772	2.307	7.0812
Compr. mod. In the transverse dir. E_{2c} [GPa]:	14.35	3.345	14.998	1.699	-4.5157
Major Poisson ratio, v_{12}:	0.36	33.33	0.291	9.33	19.1667
Tensile strength along the fiber, X [MPa]:	802.75	2.57	776.497	4.655	3.2704
Compress. strength along the fiber, X' [MPa]:	686.32	8.67	521.822	3.162	23.9681
Tensile strength transv. to the fiber, Y [MPa]:	55.08	4.865	53.9516	4.775	2.0487
Compress. strength transv. to the fiber, Y' [MPa]:	161.7	5.529	165.004	2.938	-2.0433
Tensile strain at failure along the fiber, ε_{1T} (%)	2.53	15.81	2.0913	4.583	17.3399
Tensile strain at failure transv. to the fiber, ε_{2T} (%)	0.48	8.333	0.4216	8.9106	12.1667
Compress. strain at failure along the fiber, ε_{1C} (%)	1.84	9.783	1.406	4.934	23.5870
Compress. strain at failure transv. to the fiber, ε_{2C} (%)	2.12	12.26	1.998	8.2686	5.754717

Table 3. S-N curve definitions for in-plane material characterization

∥	R	σ_o	k
	-1	1059.659	8.04
	0.1	556.108	9.743
	10	247.5	58.823

$$\sigma_a = \sigma_o N^{\left(-\frac{1}{k}\right)} \quad in \quad [MPa]$$

$$\tau_a = \tau_o N^{\left(-\frac{1}{k}\right)} \quad in \quad [MPa]$$

⊥	R	σ_o	k
	-1	87.52	8.432
	0.1	50.211	8.631
	10	88.5465	24.32
Shear	**R**	**τ_o**	**k**
	0.1	53.82638	11.06

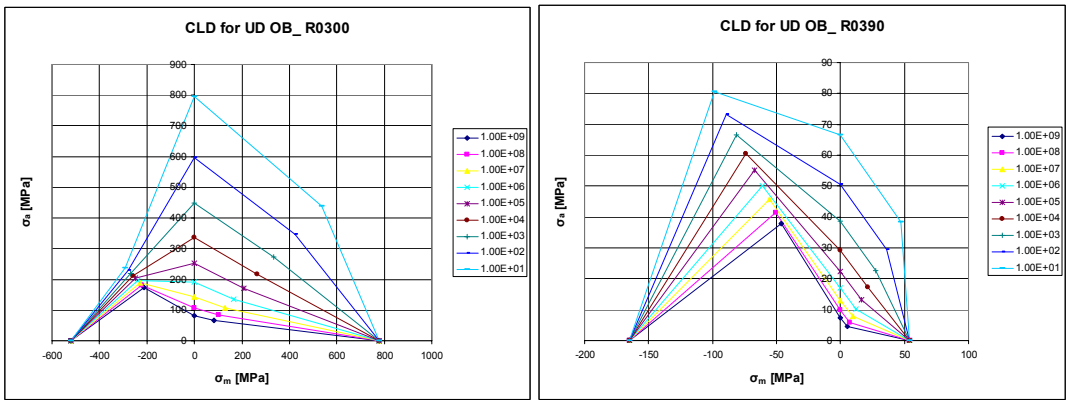

Fig.1 Constant Life Diagrams for OB UD material along and transverse to the fiber

It is believed that the database created for the in-plane characterization of the UD material can be used for similar epoxy laminates if a single batch of 'confidence' testing for a material combination gives similar results.

3. Complex stress states in a rotor blade

A rotor blade even if loaded in a complex mode, it is after all a thin-wall beam structure. As such, the tangential stress resultant in the shell thickness is negligible compared to the axial one. However, the shear stress resultant is of comparable magnitude to the axial one in areas as the shear webs or trailing and leading edges respectively. If the different strength values in the axial direction and in shear are also taken into account, it makes it easier to understand the importance of the combined effect of these actions. An example is given in Fig.2 where stress results from a transition section of a 30m blade are presented.

The above described situation implies a pure complex stress-state at the ply level; see Fig.3 where stress analysis results from a 35m blade are presented. It is clearly seen that in the plies with fibers oriented in the blade axis, normal stress transverse to the fibers and shear stress are negligible compared to the normal axial stress. However, in plies with fibers oriented at + or -45 the prevailing stress field is complex.
In conclusion, 1D stress analysis, i.e. beam theory formulations, could be acceptable but failure prediction should be done in a layer-by-layer basis, i.e. complex stress states at the ply level should be taken into account. Whatever is the type of stress analysis, i.e. beam or shell implementations, provided that failure occurrence is accounted properly, the level of safety (reliability) is increased when taking into account complex stress states (…indicating a possible reduction in the product, γ_m, of partial safety factors; GL and DNV have been considering this in their latest design guidelines editions)

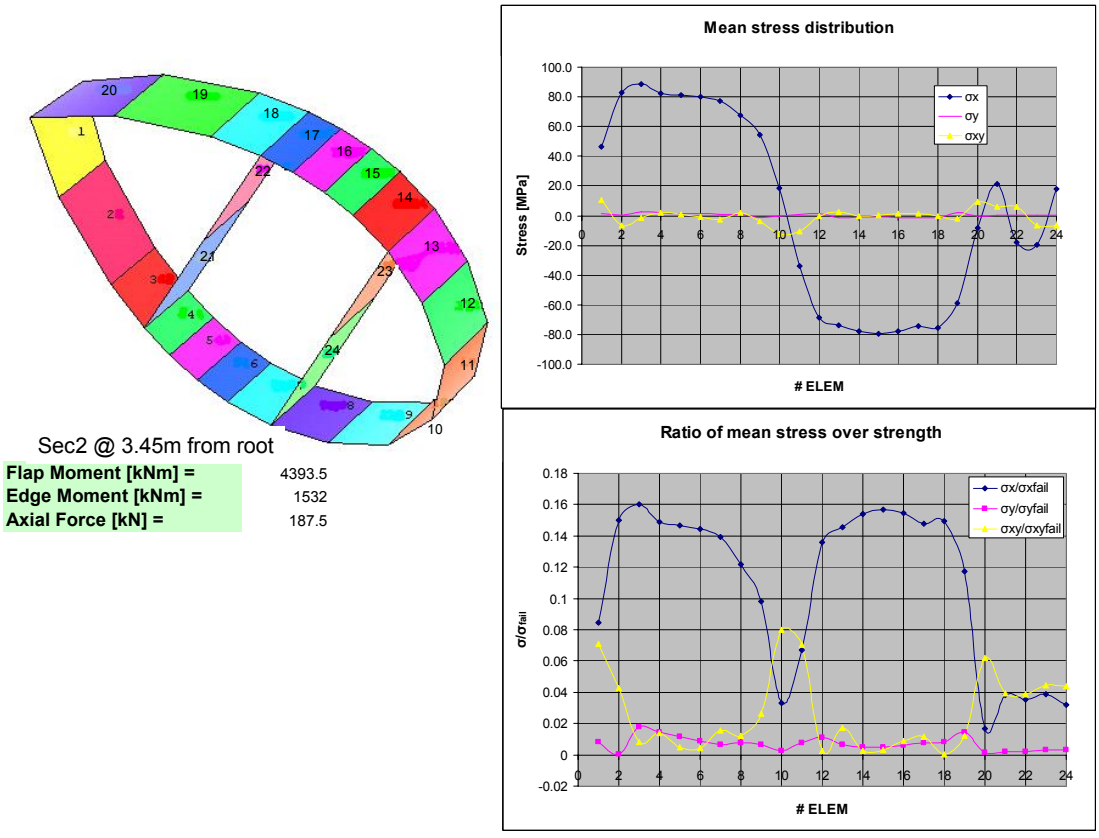

Fig.2. Typical stress state in a transition section of a 30m blade. σ_x, σ_y and σ_{xy} stand for the normal stress resultants in the axial, tangential directions and the shear stress resultant respectively.

Nose	Layer 1		Layer 2		Layer 3		Layer 4
	+45(2)	-45(2)	+45(2)	-45(2)	+45(5)	-45(5)	0(6)
σ_1 [MPa]	-25.706	-30.025	-26.418	-30.572	-29.413	-33.466	-70.200
σ_2 [MPa]	-8.795	-7.954	-8.968	-8.160	-11.934	-10.901	2.170
σ_6 [MPa]	14.822	-14.822	14.635	-14.635	13.045	-13.045	0.371

Tail	Layer 1		Layer 2		Layer 3	
	+45(2)	-45(2)	+45(2)	-45(2)	+45(2)	-45(2)
σ_1 [MPa]	74.013	77.732	64.219	65.298	44.572	40.355
σ_2 [MPa]	23.165	22.441	19.568	19.358	12.352	13.173
σ_6 [MPa]	-26.015	26.015	-28.229	28.229	-32.669	32.669

Spar	Layer 1		Layer 2	Layer 3	
	+45(2)	-45(2)	0(8)	+45(2)	-45(2)
σ_1 [MPa]	-59.825	-66.360	-109.550	-19.758	-10.888
σ_2 [MPa]	-19.598	-18.326	1.388	-3.742	-5.468
σ_6 [MPa]	10.589	-10.589	-0.147	21.895	-21.895

Web	Layer 1		Layer 2	Layer 3	
	+45(5)	-45(5)	foam	+45(5)	-45(5)
σ_1 [MPa]	-26.998	26.700	-0.003	-45.078	41.206
σ_2 [MPa]	6.790	-6.899	0.001	10.295	-11.701
σ_6 [MPa]	0.802	-0.802	-0.041	0.490	-0.490

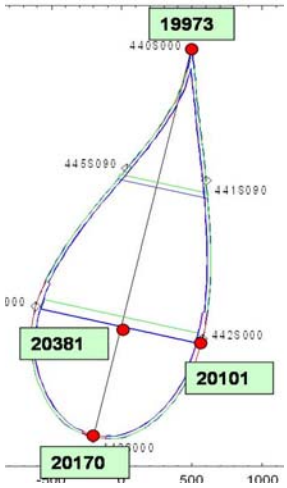

Section at 7m from root
(largest chord)

4500 **kNm and** -990 **kNm**

Fig.3. Ply stress analysis in the largest chord section of a 35m blade.

4. Failure prediction under complex stress states

Typical plane stress states as those developed in the layers of the shells shown in Fig.3 can be simulated, besides sophisticated biaxial tests, by uniaxial testing in off-axis UD coupons, see Fig.4. Failure prediction under static loading is performed satisfactorily using criteria such as Tsai-Wu, Puck and Tsai-Hill as shown in Fig.5. Under cyclic loading, life prediction is also satisfactorily performed when using similar quadratic in stress functions compared to simplistic approaches, such as to consider separately damage from each stress component and add at the end. An example of such an exercise is shown in Fig.6 where algorithm details are presented. In Fig.7, test results from off-axis loaded UD coupons, at 10^o, are compared to theoretical predictions from the two different approaches.

Experimental results from cyclic biaxial tests, using specimens either of cruciform or tubular geometry, are not yet available or processed. Static tests results from bi-axial tension of cruciform specimens made of MD lay-up suggest that failure prediction according to limit functions as those cited in the above is fair, in general, although many other parameters such as stiffness degradation scenarios or material non-linearity for example are of paramount importance. An example of such a comparison is presented in Fig.8, where test results from cruciform specimens [OB_TG2_R016] are plotted along with theoretical predictions from various failure criteria as Puck, Tsai-Hahn or EPFS (Elliptic Paraboloid Failure Surface thought as a generalization of Hoffmann anisotropic failure criterion).

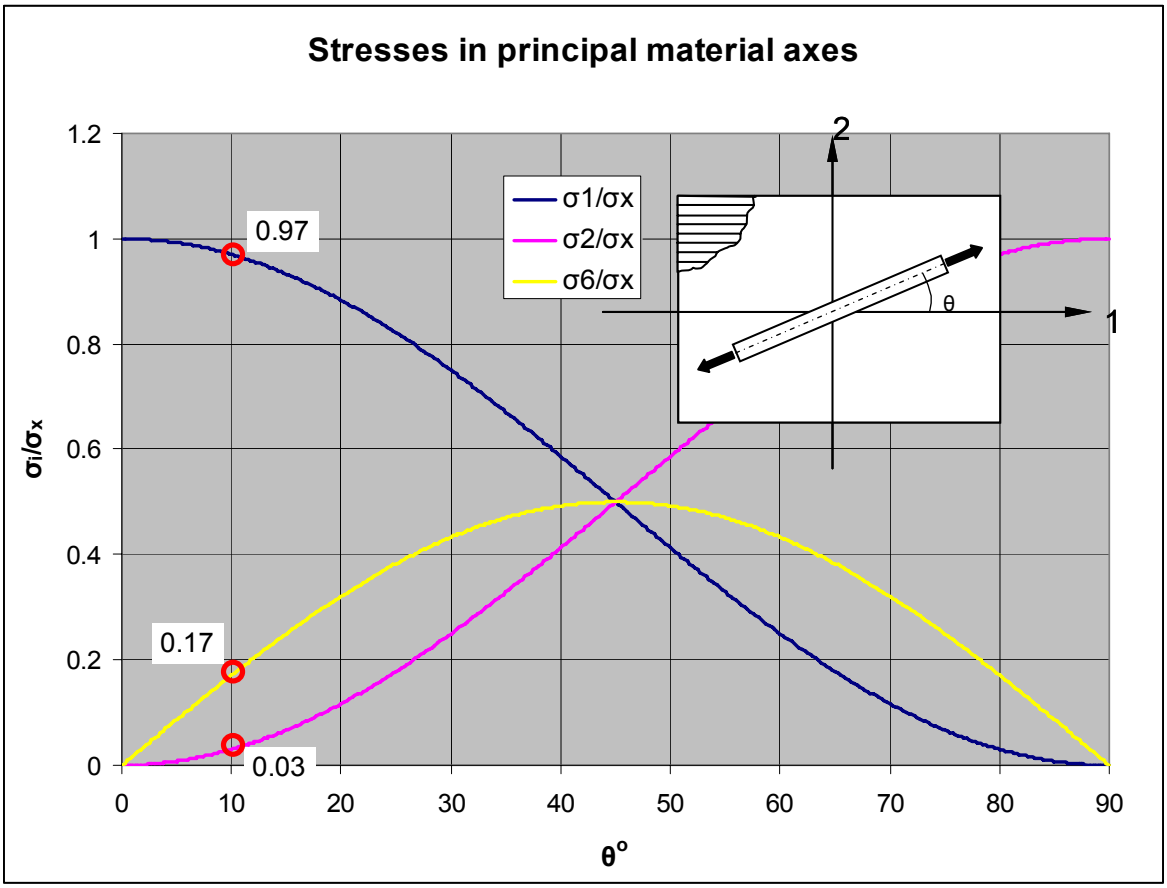

Fig.4. Off-axis loading UD coupons

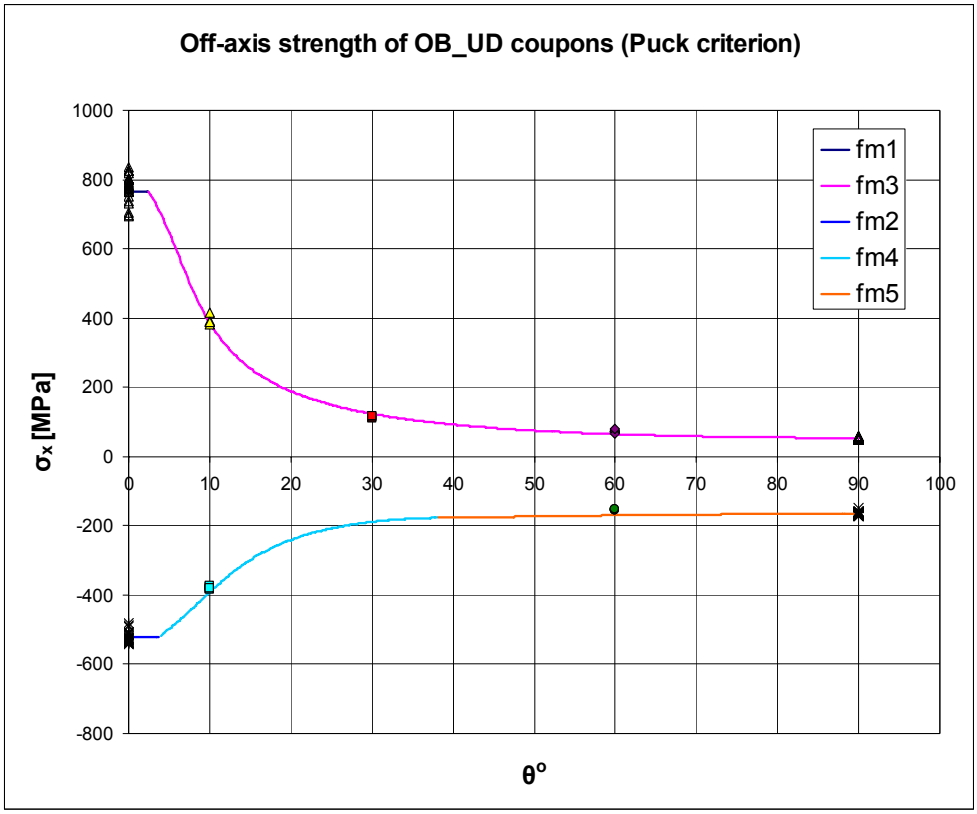

Fig.5. Experimental verification from off-axis loaded OB_UD coupons

Fatigue analysis

Simple approach

$$\sigma_{ia} = \sigma_{io} N^{-\frac{1}{k_i}}, \quad i = 1,2,6 \quad \Rightarrow \quad N = \left(\frac{\sigma_{ia}}{\sigma_{io}}\right)^{-k_i}$$

$$\sigma_{1a} = \sigma_{xa}\cos^2\theta$$
$$\sigma_{2a} = \sigma_{xa}\sin^2\theta$$
$$\sigma_{6a} = \sigma_{xa}\sin\theta\cos\theta$$

$$D_1 + D_2 + D_6 = 1$$

$$n = \frac{1}{\left(\frac{\sigma_{1_a}}{\sigma_{1_o}}\right)^{k_1} + \left(\frac{\sigma_{2_a}}{\sigma_{2_o}}\right)^{k_2} + \left(\frac{\sigma_{6_a}}{\sigma_{6_o}}\right)^{k_6}}$$

Tsai-Hill

$$\left(\frac{\sigma_{1_a}}{\sigma_{1_o} n^{-\frac{1}{k_1}}}\right)^2 + \left(\frac{\sigma_{2_a}}{\sigma_{2_o} n^{-\frac{1}{k_2}}}\right)^2 + \left(\frac{\sigma_{6_a}}{\sigma_{6_o} n^{-\frac{1}{k_6}}}\right)^2 - \frac{\sigma_{1_a}\cdot\sigma_{2_a}}{\left(\sigma_{1_o} n^{-\frac{1}{k_1}}\right)^2} = 1$$

Solving for n

Fig.6 Algorithms for life prediction under complex stress states; a simplistic approach and the use of a non-linear function derived by generalizing the Tsai-Hill limit function

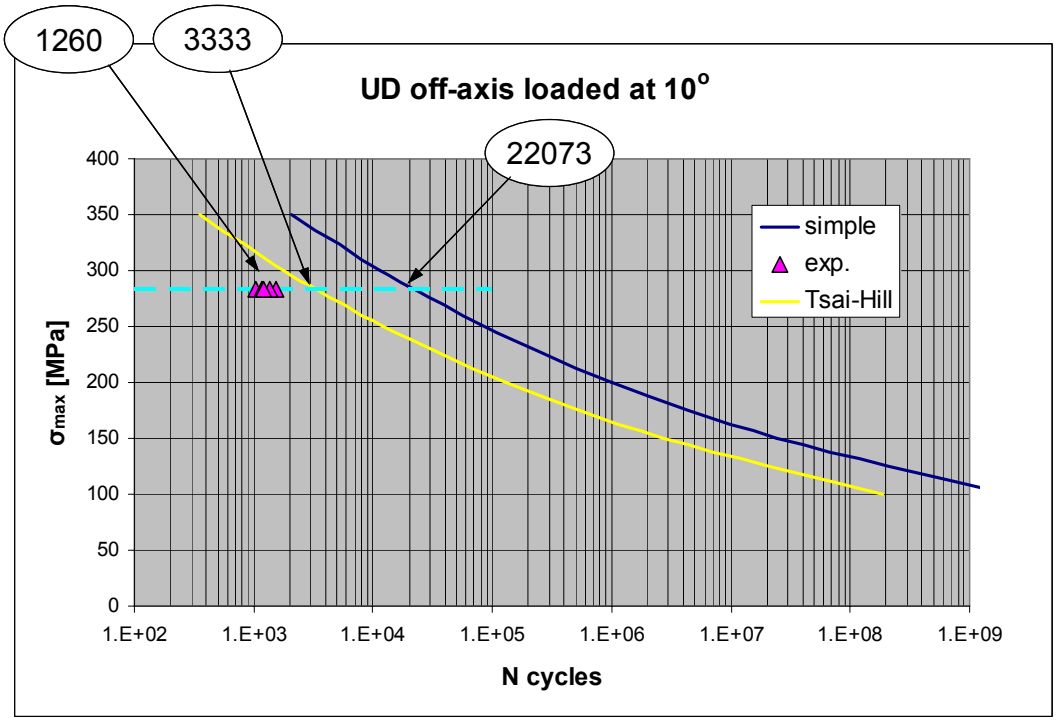

Fig.7 Experimental verification from off-axis loaded OB_UD coupons

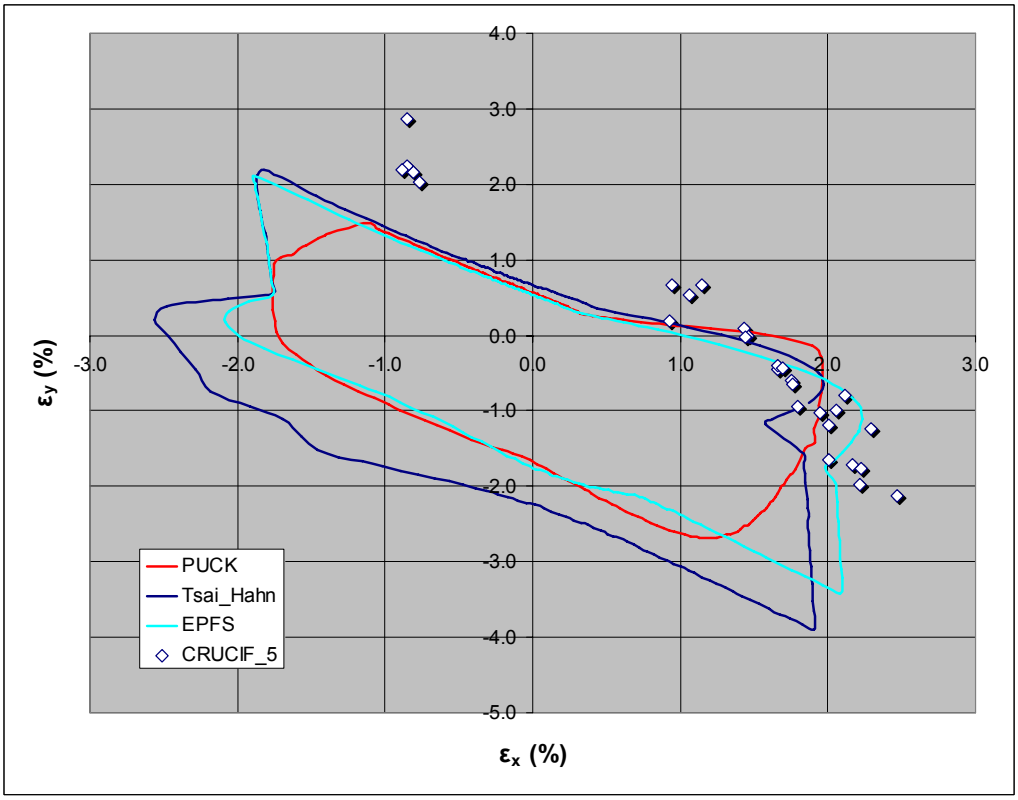

Fig.8 Comparison of test results from bi-axial testing of cruciform specimens and theoretical predictions from various failure criteria